HHS Public Access

Author manuscript

Neurobiol Aging. Author manuscript; available in PMC 2024 September 27.

Published in final edited form as:

Neurobiol Aging. 2021 March ; 99: 1–10. doi:10.1016/j.neurobiolaging.2020.11.014.

Longitudinal changes in network homogeneity in presymptomatic C9orf72 mutation carriers

Rebecca E. Waugh,

Laura E. Danielian,

Rachel F. Smallwood Shoukry,

Mary Kay Floeter

National Institute of Neurological Disorders and Stroke, National Institutes of Health Bethesda MD 10 Center Drive 20892-1140 USA

Abstract

The risk for carriers of repeat expansion mutations in C9orf72 to develop amyotrophic lateral sclerosis and frontotemporal dementia increases with age. Functional magnetic resonance imaging studies have shown reduced connectivity in symptomatic carriers, but it is not known whether connectivity declines throughout life as an acceleration of the normal aging pattern. In this study, we examined intra-network homogeneity (NeHo) in 5 functional networks in 15 presymptomatic C9+ carriers over an 18-month period and compared to repeated scans in 34 healthy controls and 27 symptomatic C9+ carriers. The longitudinal trajectory of NeHo in the somatomotor, dorsal attention, and default mode networks in presymptomatic carriers differed from aging controls and symptomatic carriers. In somatomotor networks, NeHo increased over time in regions adjacent to regions where symptomatic carriers had reduced NeHo. In the default network, the posterior cingulate exhibited age-dependent increases in NeHo. These findings are evidence against the proposal that the decline in functional connectivity seen in symptomatic carriers represents a lifelong acceleration of the healthy aging process.

Keywords

Amyotrophic lateral sclerosis; *C9orf72* ; frontotemporal dementia; functional connectivity; presymptomatic carrier; resting-state fMRI

Corresponding author Mary Kay Floeter floeterm@ninds.nih.gov Alternate email: floetermk@gmail.com, 10 Center Drive MSC 1140, Bethesda MD 20892-1140, 301-451-9805 (f).

Declaration of interest: none

Disclosure statement

The authors have no conflicts of interest to disclose. CRediT authorship contribution statement: Rebecca E. Waugh: Writing - original draft, Formal analysis, Methodology, Visualization. Laura E. Danielian: Investigation, Formal analysis, Writing - review & editing. Rachel F. Smallwood Shoukry: Investigation, Writing - review & editing. Mary Kay Floeter: Supervision, Conceptualization, Writing - review & editing.

1. INTRODUCTION

The C9orf72 repeat expansion mutation is one of the most common causes of familial amyotrophic lateral sclerosis (ALS) and frontotemporal dementia (FTD) (DeJesus-Hernandez et al., 2011; Renton et al., 2011). For C9orf72 repeat expansion carriers (termed C9+ carriers), the risk of developing symptoms of a neurodegenerative disorder increases with age. Although the median age of symptom onset is 58 years, some C9 carriers are diagnosed as early as the third decade of life, while others remain symptom-free much longer (Murphy et al., 2017). Although older age is a risk factor for developing disease in C9 carriers, the heterogeneity of age at onset complicates studying the relationship between the trajectory of disease and healthy aging. Understanding whether aging interacts with the mutation to affect the onset and progression of clinical symptoms may provide useful information for determining the timing for initiating interventional treatments.

Neurodegenerative diseases are known to alter functional and structural brain networks (Filippi et al., 2019; Seeley et al., 2009; Seeley 2017). Functional networks, characterized by temporal correlation of activity among widespread brain regions (Biswal et al., 1995; Fox et al., 2005) are intrinsically organized, remain stable in task-free settings (Fox et al., 2005), and reflect underlying neuroanatomy (van den Heuvel et al., 2009). However, network organization changes across the lifespan. In healthy adults, intra-network functional connectivity (FC) decreases with age, while inter- network FC increases (Betzel et al., 2014). The healthy aging pattern reportedly differs in sporadic ALS patients, with increasing FC with age in the posterior cingulate cortex in the default mode network (DMN; Tedeschi et al., 2012). Another study of age-related changes in FC in a cohort of presymptomatic C9+ carriers found that patterns of altered connectivity were similar to those of symptomatic carriers, and did not accelerate with age (Lee et al., 2017). Such studies with cross-sectional designs make it difficult to disentangle age from individual differences in disease progression. Cohorts of presymptomatic carriers have a highly variable (and unknown) number of years until disease onset, and inter- individual differences may mask connectivity changes related to disease progression.

In this study, we followed a cohort of presymptomatic and symptomatic C9+ carriers longitudinally over a period of 18 months, focusing on changes in functional networks over that time period. We had previously found that certain regions, particularly the posterior cingulate and parietal cortex, exhibited altered FC within multiple networks which were defined using seed-based methods (Shoukry et al., 2020). Because seed-based analysis evaluates connectivity only to the selected seed regions, it cannot characterize the entire pattern of connectivity within networks. Homogeneity is a summary measurement of intra-network FC in task-free functional magnetic resonance imaging (fMRI) (Uddin et al., 2008). By calculating both the voxel-wise homogeneity and the homogeneity of the network as a whole (NeHo), an assessment of the overall state of the network and its component regions is possible. Although not an exhaustive list of potential networks, we chose 5 networks of interest based on prior evidence for functional alterations in ALS patients, including motorrelated (Agosta et al., 2011; Chenji et al., 2016; Douaud et al., 2011; Jelsone-Swain et al., 2010; Lulé et al., 2007, 2009; Mohammadi et al., 2009; Zhou et al., 2013), attention and salience-related (Schulthess et al., 2016; Trojsi et al., 2015), DMN (Agosta et al., 2012;

Chenji et al., 2016; Mohammadi et al., 2009), and frontoparietal network (FPN; Agosta et al., 2012, 2013; Menke et al., 2016).

The study aimed to investigate the character and trajectory of aging in C9+ mutation carriers in these networks. Characterizing how neurodegeneration interacts with aging and deviates from healthy age-related changes is an important step in understanding the C9+ disease trajectory. This study addresses 2 questions: (1) Does C9-related neurodegeneration accelerate healthy aging processes in functional networks or deviate qualitatively from the aging trajectory? (2) Do changes in connectivity networks in C9+ carriers exhibit a stable linear trend over time or do the changes occur more suddenly in the period just before disease onset?

2. METHODS

2.1. Participants

MRI scanning was carried out on 42 carriers of C9orf72 expansion mutations (C9+ carriers) and 34 healthy control subjects (HC) who gave written informed consent for protocols approved by the National Institutes of Health Institutional Review Board (NCT01925196 and NCT01517087). The demographic features and clinical evaluations of these cohorts have been previously described (Floeter et al., 2017; Shoukry et al., 2020). In brief, all C9+ carriers had >30 repeats in C9of72 by testing in Clinical Laboratory Improvement Amendments (CLIA) certified laboratories. All but two C9+ carriers were unrelated (of whom one was presymptomatic). Fifteen C9+ carriers had no clinical symptoms of disease at enrollment. Of the 27 symptomatic C9+ carriers, 17 had ALS, 6 had ALS-FTD, and 4 had dementia at enrollment. All C9+ carriers had clinical and imaging measures at baseline with followup clinical evaluations and scanning scheduled 6 and 18 months later. Longitudinal scans were obtained in all presymptomatic C9+ carriers and 22 healthy subjects. Cognitive and motor function measures showed no decline over time in presymptomatic C9+ carriers, including measures of letter fluency, as previously reported (Shoukry et al., 2020). Because many symptomatic C9+ carriers were unable to undergo longitudinal scans, cross-sectional analyses using the last scan obtained for each C9+ carrier were included. Table 1 provides the demographics and timing of scans for all groups.

2.2. MRI acquisition

MRI scans were acquired using methods previously described for anatomical, diffusion tensor, and functional resting-state imaging (Floeter et al., 2016, 2018; Shoukry et al., 2020). Briefly,scans were collected between 2012 and 2019 on 3T GE HDX and GE 750 scanners (GE Medical Systems, Milwaukee, WI). Scans included 2 high-resolution T1 scans for anatomical structure and for registration (resolution 256 256, voxel size 1 0.938 0.938 mm, 140e176 slices), multi-slice diffusion weighted images using a single-shot spin-echo echo-planar sequence (field of view (FOV) 240 240, resolution 96 96, 64 axial slices, 2.5-mm slice thickness) with a total of 80 diffusion volumes (70 directions diffusion weighting with 10 volumes at b 1/4 300 s/mm^2 and 60 volumes at b 1/4 1100 s/mm^2 and 10 b(0) volumes), and a resting-state functional MRI (echo time (TE) 30 ms, repetition time (TR) 2s, FOV 240 240, resolution 64 64, voxel size 3.75 3.75 3.8 mm, 40 slices). The resting-state

functional MRI (rs-fMRI) scan lasted approximately 8 minutes with eyes open and fixation on a centered onscreen cross.

2.3. Image processing

2.3.1. Resting-state fMRI—Preprocessing steps were conducted with analysis of functional imaging (AFNI) software (Cox 1996) and included clipping the first 4 volumes, despiking, motion correction, spatial smoothing (full width at half-maximum kernel size 1/4 5 mm) and intensity normalization. White matter (WM), gray matter (GM), and cerebrospinal fluid (CSF) masks were derived by skull stripping and segmenting the anatomical T1 image. With these masks, mean functional activity time courses for each region in the resting-state scan were generated. WM and CSF time courses, 6 motion parameters and their derivatives, and a high-pass temporal filter comprised the nuisance covariates in a regression model of the data, whose function was to estimate the normalized functional data without these sources of physiological noise (Birn 2012). Each subject's T1 image was registered to the MNI152 2-mm standard brain using a 2-step process of affine alignment followed by non- linear warping.

2.3.2. Diffusion tensor imaging—Diffusion weighted images were pre-processed using the TORTOISE software package (https://science.nichd.nih.gov/confluence/display/nihpd/TORTOISE), including correction of motion artifacts and eddy current distortion, calculation of the tensor, and DTI metrics of fractional anisotropy (FA), mean diffusivity, axial diffusivity, and radial diffusivity. FA and mean diffusivity maps from different scanners were adjusted using ComBat (Fortin et al., 2017). A voxel-wise comparison of whole-brain FA skeletons of the C9+ and control groups was carried out in Tract-Based Spatial Statistics (v1.2, http://www.fmrib.ox.ac.uk/fsl/) using the methods of Smith et al. (2006). The most "typical" subject in the study was chosen by Tract-Based Spatial Statistics as the target image for registration. A threshold of 0.2 was used to create the mean FA skeleton (Smith et al., 2006). Images were visually inspected in all registered brains to confirm a good representation of the core WM tracts. Contrasts were performed using the Randomise tool in FSL (v2.9, 5000 permutations), with gender and age as covariates. Significant clusters were determined using Threshold-Free Cluster Enhancement at $p < 0.05$ corrected for multiple comparisons across space (family- wise error (FWE)).

2.3.3. Cortical thickness and volume measurement—The FreeSurfer v6.0.0 image analysis suite (http://surfer.nmr.mgh.harvard.edu/) was used for cortical reconstruction and volumetric segmentation of presymptomatic C9+ carriers, as described in prior publications (Fischl et al., 1999, 2002, 2004), including our prior report on symptomatic C9+ carriers (Floeter et al., 2016). Briefly, the processing included skull stripping, Talairach trans- formation, optimization of the GM-WM and GM-CSF boundaries, and segmentation. After visual inspection and manual correction for errors in segmentation, tessellated surfaces were inflated and registered to a spherical atlas for parcellation of the cerebral cortex into 34 regions in each hemisphere (Desikan et al., 2006). The FreeSurfer longitudinal stream, which creates an unbiased within- subject template for measuring changes in cortical thickness over time (Reuter et al., 2012), was used. The FreeSurfer QDEC tool was used to carry out whole-brain vertex-wise comparisons between groups of

presymptomatic C9+ carriers and controls. Data were smoothed at 10 mm, and $p < 0.05$ with false discovery rate (FDR) correction was used as criteria for significance.

2.4. Calculating brain connectivity measures restricted within networks

Network parcellation maps were created by applying the 7-network solution of Yeo et al. (2011) in MNI152 2-mm space to the GM-only functional data. Five of these networks were hypothesized to be networks of interest, and these were deployed to produce functional data sets restricted to these networks of interest (dorsal attention network [dAN], DMN, FPN, somatomotor network [SMN], and ventral attention network [vAN]).

Voxel-wise homogeneity was calculated with the following equation derived from Uddin et al. (2008)

$$NeHo_i = \sum_{j=1}^{n} \frac{r(TS_i, TS_j)}{n-1} \text{ where } i \neq j$$

The time series (TS) of each voxel in the network served as a seed and the Pearson's correlation was computed with every other voxel TS in the network. For every voxel i, we calculated the mean of all the correlations for voxels j through n 1, where n is the total number of voxels in the network. The resulting voxel-wise NeHoi is assigned to voxel i's position in a new statistical map. To calculate the summary NeHo measure for each network, the voxel-wise homogeneity measurements were summed to create a single weighted value of network homogeneity for each subject at each timepoint. To get a complete picture of the network, we did not threshold by the magnitude of correlation nor exclude anti-correlations. To facilitate direct comparison between the networks of interest, NeHo was divided by the total number of voxels in the network.

2.5. Statistical modeling

A linear mixed effects model using R software (RStudio, v1.3.959) was used to assess differences in NeHo between groups across the networks of interest. Each subject contributed one value for each network. For the cross-sectional analysis, the last scan collected up to the 18-month timepoint was used for each subject. Differences between groups and networks were tested, along with the relationship to subject age. We did not include sex as a covariate because sex was highly collinear with presymptomatic C9+ status. Scanner type was included as a nuisance covariate. We conducted an additional linear mixed effects model with all scans collected up to the 18-month timepoint for the 5 networks of interest to investigate longitudinal changes in NeHo over the course of the study.

To determine whether particular regions within each network of interest contributed to the group differences seen in NeHo, an additional set of analyses on the voxel-wise homogeneity statistical maps were carried out in AFNI, using the same cross-sectional cohort, with age and scanner type as covariates. Additionally, to assess longitudinal changes, a linear mixed effects analysis (Chen et al., 2013) of these maps was carried out on all scans up to the 18-month visit where age, months since baseline scan, and the 2- and 3-way interactions with subject group were parameterized, with scanner type as a nuisance

covariate. To reveal any significant regions, we first applied a whole-brain voxel-wise threshold of $p < 0.001$ uncorrected to the resulting outputs for the parameters of interest: subject condition, and the interactions among condition, age, and time. AFNI's 3dClustSim was then used to estimate the required number (k voxels, NN 1/4 1) of proximate significant voxels to reach an FWE-corrected significance threshold of $p < 0.05$.

3. RESULTS

3.1. Cross-sectional comparisons between groups at last timepoint

3.1.1. Group differences in NeHo—The scans obtained at the last timepoint for each subject were used to compare mean network homogeneity (NeHo) between groups for the 5 networks. There was a significant difference in the NeHo between groups (F 1/4 9.99, $p <$ 0.001). A Tukey's post hoc test comparing each of the 3 cohorts by network showed a linear trend with greatest homogeneity in healthy controls and least homogeneity in symptomatic C9+ subjects in 4 networks: dAN, DMN, SMN, and vAN (Fig. 1). There were no significant differences between any groups in FPN.

3.1.2. Voxel-wise comparisons between controls and C9+ carrier groups—Symptomatic C9+ carriers had localized regions with reduced homogeneity within several networks compared to healthy controls ($p < 0.05$, FWE-corrected; Fig. 2, red regions). The SMN had the most regions with reduced homogeneity, that is, greatest percentage of voxels with significant reductions in voxel-wise homogeneity, followed by the DMN. Regions with reduced connectivity in the dAN, FPN, and vAN were much smaller (Table 2). In presymptomatic C9+ carriers, only small localized regions within the SMN, DMN, and dAN had reduced homogeneity compared to healthy controls. These consisted of substantially fewer voxels than in the symptomatic C9+ carriers (Table 2). These regions included the right precentral and right medial frontal cortex in the SMN, the left superior parietal region in the DMN, and the right middle temporal region in the dAN. These reduced regions overlapped (Fig. 2, yellow color) or were in close proximity (Fig. 2, blue regions) to the regions affected in symptomatic C9+ carriers. There were no regions in the FPN and vAN with significant reductions in pre- symptomatic C9+ carriers. Neither C9+ carrier group had regions with increased homogeneity in any network compared to healthy controls.

3.2. Longitudinal analyses

3.2.1. Age-related longitudinal changes in NeHo in all groups—Age-related longitudinal changes in NeHo differed among the 3 diagnostic groups (F 1/4 2.45, p 1/4 0.013). Presymptomatic C9+ carriers had significantly less age-related reduction in NeHo compared to healthy controls and symptomatic subjects in SMN and dAN ($p <$ 0.05; Fig. 3A). In these networks the NeHo was stable or slightly increased with age in presymptomatic C9+ carriers. Increased NeHo with age also approached significance in the FPN (p 1/4 0.064; Fig. 3A).

3.2.2. Longitudinal changes in voxel-wise homogeneity in presymptomatic C9+ carriers—In the 15 presymptomatic carriers, several regions in the SMN had increasing homogeneity over time, including in the left and right precentral and postcentral

gyri, right insula, left superior temporal gyrus, and the cingulate, spreading left and right from midline (Fig. 4A). This increase was time, but not age, dependent. These regions were adjacent to, but rarely overlapping, areas found to have reduced connectivity in symptomatic carriers at the final timepoint in the cross-sectional comparison (Fig. 4B). The longitudinally increasing homogeneity in these regions of SMN was largely derived from a reduction in the number of anti-correlated voxels, coupled with stronger correlations of positively correlated voxels to the network as a whole (Table 3).

3.2.3. Age-related changes in voxel-wise homogeneity in presymptomatic C9+ carriers—Regions within 4 of the networks exhibited a different age- related trajectory of homogeneity changes in presymptomatic C9+ carriers compared to healthy controls (Fig. 3B). In 4 regions in the SMN, dAN, DMN, and FPN, the mean homogeneity increased with age in presymptomatic C9+ carriers but declined with age in healthy controls. One small region in the FPN (Fig. 3B, FPN2) exhibited the opposite trend, increasing with age in healthy controls and declining in presymptomatic C9+ carriers. Only one region showed a significant interaction between age and time. In the left posterior cingulate the rate of the increase in mean homogeneity in the DMN increased with age (Fig. 5).

3.2.4. Longitudinal changes in white matter in presymptomatic C9+ carriers—Presymptomatic C9+ carriers showed no WM areas with significantly different diffusion indices from healthy controls when comparing their first and last scans. However, the presymptomatic C9+ carriers had 2 small WM regions, one near the genu of the internal capsule and the other in the callosum, with increased axial diffusivity between their first and last scans (Fig. 6).

3.2.5. Cortical thickness and volumes—There were no significant differences in measures of cortical volumes or thickness between presymptomatic C9+ carriers and healthy controls. Rates of thinning (symmetrized percent change) of different cortical regions did not differ from controls in longitudinal scans. There was no significant interaction between age and C9+ carrier status in presymptomatic carriers.

4. DISCUSSION

FC of several cortical networks was reduced in patients with ALS and/or FTD caused by the C9orf72 expansion mutation. Loss of intra-network homogeneity resulted from regions within networks whose activity was less correlated to the rest of the network. The SMN and DMN networks were particularly affected in these symptomatic C9+ carriers. However, as the symptomatic carriers aged, the rate of decline in network homogeneity mostly paralleled the normal aging trajectory. In contrast, presymptomatic C9+ carriers presented a different pattern of abnormal homogeneity compared to healthy controls. In the presymptomatic C9+ carrier group, network homogeneity was less than in controls, but the SMN, dAN, and FPN did not follow the trajectory of decline seen with normal aging. Younger presymptomatic C9+ carriers had lower homogeneity than older presymptomatic C9+ carriers in the SMN and dAN, with increasing homogeneity in subregions of these networks and the DMN over the 18-month follow-up. This suggests that the neurodegenerative processes captured by functional alterations in C9+ subjects are not simply the straightforward product of

accelerated aging. Although age is predictive of symptom onset (Murphy et al., 2017) these divergent trajectories support the proposal that networks begin to lose FC at the onset, or shortly before, emergence of clinical symptoms, rather than exhibiting a gradual, but accelerated, decline with age.

Our longitudinal findings highlight the complex dynamics of network connectivity throughout disease progression. Prior fMRI studies in patients with ALS have reported both increases and decreases in FC, particularly in motor cortex networks (Agosta et al., 2013; Douaud et al., 2011; Jelsone-Swain et al., 2010; Loewe et al., 2017; Menke et al., 2016, 2018; Mohammadi et al., 2011; Stanton et al., 2007). Although methodological differences in analysis can account for some differences in findings, this mixed picture could very well reflect differences in the stage of disease progression (Agosta et al., 2011; Menke et al., 2018). In presymptomatic C9+ carriers we found that small regions within the SMN, which were adjacent to those areas with decreased FC in symptomatic C9+ carriers, developed increasing FC over time. These regions with increased intra-network connectivity may be a prodrome to detectable neurodegeneration. This interpretation would be consistent with work by Agosta et al. (2017) who proposed that increasing FC may be among the earliest detectable abnormalities as disease progresses, followed by declining connectivity when structural damage exceeds a certain threshold. Alternatively, increased FC could reflect a transient compensation, recruiting regions distant from areas with subtle structural damage. Notably, despite close proximity, there was relatively little overlap between the affected regions in symptomatic patients and the areas that saw increases in presymptomatic C9+ carriers. In our study, the enhanced FC in the SMN of presymptomatic C9+ carriers resulted from recruitment of small previously unconnected or less connected regions, including anti-correlated regions, causing the network as a whole to be more homogeneous and less differentiated. A similar result has been found in sporadic ALS patients, where short-range FC in the motor network was reduced while longer range connections, including to motor regions beyond the precentral gyrus were enhanced (Konrad et al., 2002; Li et al., 2018; Sorrentino et al., 2018). This pattern of subtle, but not age- dependent, decline in the homogeneity of the network may depend on the recruitment of these proximate regions, serving to preserve network function against incipient damage. Such changes could allow network efficiency to be maintained despite declining functional connections until reaching a threshold that coincides with symptom onset, as proposed for presymptomatic carriers of FTD genes (Rittman et al., 2019).

We previously reported that posterior parietal and cingulate cortex regions had reduced FC in several seed-based networks in symptomatic C9+ carriers, including the motor and salience network (Shoukry et al., 2020). This study found that the posterior cingulate cortex had faster increases in connectivity in the DMN with age in presymptomatic C9+ carriers, in contrast to declining FC in controls. Older presymptomatic C9+ carriers developed marked increases in connectivity compared to younger subjects, even over the relatively short time period of the study. Tedeschi et al. (2012) similarly noted that FC increased with age in the posterior cingulate in the DMN in ALS patients, and declined with age in controls. The posterior cingulate may be a particularly key region in compensating for encroaching cognitive dysfunction. Structurally, it has reciprocal connections with temporal and frontal

cortices, and is postulated to play a role in regulating the focus of attention (Leech and Sharp, 2014).

Subtle abnormalities in brain structure, cognition, and psychiatric changes have been detected in large cohorts of familial carriers of FTD genes years or even decades prior to the age of predicted onset (Bertrand et al., 2018; Caverzasi et al., 2019; Devenney et al., 2018; Lee et al., 2017; Papma et al., 2017; Rohrer et al., 2015). The C9orf72 mutation has been postulated to affect neurodevelopment in addition to causing neurodegeneration (Caverzasi et al., 2019; Lulé et al., 2020). However, no significant atrophy was seen in the presymptomatic C9+ carriers in this study. Small regions of WM changes may represent early degeneration, but their location did not explain changes in intra-network homogeneity. The small size of our cohort of presymptomatic C9+ carriers limited our ability to detect subtle structural and cognitive differences. We did not estimate the predicted age of onset in presymptomatic C9+ carriers because we did not study affected family members nor compare presymptomatic carriers to familial controls. Of note, however, the mean age of the presymptomatic C9+ group was a decade younger than the symptomatic C9+ group and none converted over the course of the study. There was likely considerable heterogeneity in the number of years until symptom onset for these carriers, which, combined with the small sample and potentially slower disease course in women, predominant in our presymptomatic cohort, may have limited our ability to detect subtle structural differences (Rooney et al., 2017; Trojsi et al., 2019). None of the presymptomatic C9+ carriers developed symptoms during the relatively short followup time, preventing direct visualization of FC changes at the time of symptom onset. From the short-term and age-related changes in the dAN, DMN, FPN, and SMN in the presymptomatic period, we could only infer the transition to the pattern of symptomatic C9+ carriers. Our findings in symptomatic C9+ carriers differ from a previous cross-sectional study that found no differences in FC of C9+ ALS patients compared to controls (Agosta et al., 2017). The method used here, examining changes within anatomically restricted networks, differs from the whole-brain independent components analysis method used in that study. As an additional limitation, we did not have access to a group of sporadic ALS patients for comparison.

Symptom-free genetic mutation carriers have the potential to contribute substantial insights into the neurodegenerative disease process, especially in rapidly progressing diseases such as ALS (Benatar et al., 2013). Benatar et al. (2019) proposed a model for symptom development in ALS that posits a premanifest stage of disease development, in which subjects remain symptom-free even as alterations in biomarkers become detectable. Identifying periods of transition in presymptomatic genetic carriers may yield new insights into the mechanisms of disease development and the scope for intervention.

5. CONCLUSION

We found that neurodegeneration is more than a simple acceleration of the healthy aging processes in functional networks in carriers of the C9orf72 expansion mutation. During the presymptomatic period, as the carrier aged, functional activity of small regions within networks became more similar to the rest of the network, in contrast to the decline in network homogeneity in normal aging. These small regions, particularly

in the SMN, were seen adjacent to regions of the network where symptomatic C9+ carriers had decreased intra-network connectivity. The decline in network homogeneity in symptomatic C9+ carriers paralleled the decline in normal aging. We interpret the increased network homogeneity in presymptomatic C9+ carriers as a transient finding, prior to structural damage and loss of FC. Confirming this interpretation will require following presymptomatic carriers who subsequently become symptomatic to determine whether abrupt changes in functional connectivity occur with phenoconversion.

Acknowledgements

This work was supported by the Intramural Program of the National Institute of Neurological Disorders and Stroke, National Institutes of Health [Z01 NS 003146]. We are particularly grateful to the patients and healthy volunteers for their participation. We thank Ms. Jennifer Farren, RN and Ms. Carol Hoffman for assistance with coordinating patient evaluations. This work utilized the computational resources of the NIH HPC Biowulf cluster (http://hpc.nih.gov) and the Functional Magnetic Resonance Imaging Facility (https://fmrif.nimh.nih.gov).

Abbreviations

dAN	dorsal attention network
DMN	default mode network
FC	functional connectivity
FPN	frontoparietal network
$NeHo_i$	voxel-wise network homogeneity
NeHo	network homogeneity
SMN	somatomotor network
vAN	ventral attention network

References

Agosta F, Canu E, Sarro L, Comi G and Filippi M (2012). "Neuroimaging findings in frontotemporal lobar degeneration spectrum of disorders." Cortex 48(4): 389–413. [PubMed: 21632046]

Agosta F, Canu E, Valsasina P, Riva N, Prelle A, Comi G and Filippi M (2013). "Divergent brain network connectivity in amyotrophic lateral sclerosis." Neurobiol Aging 34(2): 419–427. [PubMed: 22608240]

Agosta F, Ferraro PM, Riva N, Spinelli EG, Domi T, Carrera P, Copetti M, Falzone Y, Ferrari M, Lunetta C, Comi G, Falini A, Quattrini A and Filippi M (2017). "Structural and functional brain signatures of C9orf72 in motor neuron disease." Neurobiol Aging 57: 206–219. [PubMed: 28666709]

Agosta F, Valsasina P, Absinta M, Riva N, Sala S, Prelle A, Copetti M, Comola M, Comi G and Filippi M (2011). "Sensorimotor functional connectivity changes in amyotrophic lateral sclerosis." Cereb Cortex 21(10): 2291–2298. [PubMed: 21368084]

Benatar M, Turner MR and Wuu J (2019). "Defining pre-symptomatic amyotrophic lateral sclerosis." Amyotroph Lateral Scler Frontotemporal Degener 20(5-6): 303–309. [PubMed: 30892087]

Benatar M, Wuu J and Ravits J (2013). "Opportunity and innovation in studying pre-symptomatic amyotrophic lateral sclerosis." Muscle Nerve 47(5): 629–631. [PubMed: 23494825]

Bertrand A, Wen J, Rinaldi D, Houot M, Sayah S, Camuzat A, Fournier C, Fontanella S, Routier A, Couratier P, Pasquier F, Habert MO, Hannequin D, Martinaud O, Caroppo P, Levy R, Dubois

B, Brice A, Durrleman S, Colliot O and Le Ber I (2018). "Early Cognitive, Structural, and Microstructural Changes in Presymptomatic C9orf72 Carriers Younger Than 40 Years." JAMA Neurol 75(2): 236–245. [PubMed: 29197216]

Betzel RF, Byrge L, He Y, Goni J, Zuo XN and Sporns O (2014). "Changes in structural and functional connectivity among resting-state networks across the human lifespan." Neuroimage 102 Pt 2: 345–357.

Birn RM (2012). "The role of physiological noise in resting-state functional connectivity." Neuroimage 62(2): 864–870. [PubMed: 22245341]

Biswal B, Yetkin FZ, Haughton VM and Hyde JS (1995). "Functional connectivity in the motor cortex of resting human brain using echo-planar MRI." Magn Reson Med 34(4): 537–541. [PubMed: 8524021]

Caverzasi E, Battistella G, Chu SA, Rosen H, Zanto TP, Karydas A, Shwe W, Coppola G, Geschwind DH, Rademakers R, Miller BL, Gorno-Tempini ML and Lee SE (2019). "Gyrification abnormalities in presymptomatic c9orf72 expansion carriers." J Neurol Neurosurg Psychiatry 90(9): 1005–1010. [PubMed: 31079065]

Chen G, Saad ZS, Britton JC, Pine DS and Cox RW (2013). "Linear mixed-effects modeling approach to FMRI group analysis." Neuroimage 73: 176–190. [PubMed: 23376789]

Chenji S, Jha S, Lee D, Brown M, Seres P, Mah D and Kalra S (2016). "Investigating Default Mode and Sensorimotor Network Connectivity in Amyotrophic Lateral Sclerosis." PLoS One 11(6): e0157443. [PubMed: 27322194]

Cox RW (1996). "AFNI: software for analysis and visualization of functional magnetic resonance neuroimages." Comput Biomed Res 29(3): 162–173. [PubMed: 8812068]

DeJesus-Hernandez M, Mackenzie IR, Boeve BF, Boxer AL, Baker M, Rutherford NJ, Nicholson AM, Finch NA, Flynn H, Adamson J, Kouri N, Wojtas A, Sengdy P, Hsiung GY, Karydas A, Seeley WW, Josephs KA, Coppola G, Geschwind DH, Wszolek ZK, Feldman H, Knopman DS, Petersen RC, Miller BL, Dickson DW, Boylan KB, Graff-Radford NR and Rademakers R (2011). "Expanded GGGGCC hexanucleotide repeat in noncoding region of C9ORF72 causes chromosome 9p-linked FTD and ALS." Neuron 72(2): 245–256. [PubMed: 21944778]

Desikan RS, Segonne F, Fischl B, Quinn BT, Dickerson BC, Blacker D, Buckner RL, Dale AM, Maguire RP, Hyman BT, Albert MS and Killiany RJ (2006). "An automated labeling system for subdividing the human cerebral cortex on MRI scans into gyral based regions of interest." Neuroimage 31(3): 968–980. [PubMed: 16530430]

Devenney EM, Ahmed RM, Halliday G, Piguet O, Kiernan MC and Hodges JR (2018). "Psychiatric disorders in C9orf72 kindreds: Study of 1,414 family members." Neurology 91(16): e1498–e1507. [PubMed: 30258023]

Douaud G, Filippini N, Knight S, Talbot K and Turner MR (2011). "Integration of structural and functional magnetic resonance imaging in amyotrophic lateral sclerosis." Brain 134(Pt 12): 3470–3479. [PubMed: 22075069]

Filippi M, Spinelli EG, Cividini C and Agosta F (2019). "Resting State Dynamic Functional Connectivity in Neurodegenerative Conditions: A Review of Magnetic Resonance Imaging Findings." Front Neurosci 13: 657. [PubMed: 31281241]

Fischl B, Salat DH, Busa E, Albert M, Dieterich M, Haselgrove C, van der Kouwe A, Killiany R, Kennedy D, Klaveness S, Montillo A, Makris N, Rosen B and Dale AM (2002). "Whole brain segmentation: automated labeling of neuroanatomical structures in the human brain." Neuron 33(3): 341–355. [PubMed: 11832223]

Fischl B, Sereno MI and Dale AM (1999). "Cortical surface-based analysis. II: Inflation, flattening, and a surface-based coordinate system." Neuroimage 9(2): 195–207. [PubMed: 9931269]

Fischl B, van der Kouwe A, Destrieux C, Halgren E, Segonne F, Salat DH, Busa E, Seidman LJ, Goldstein J, Kennedy D, Caviness V, Makris N, Rosen B and Dale AM (2004). "Automatically parcellating the human cerebral cortex." Cereb Cortex 14(1): 11–22. [PubMed: 14654453]

Floeter MK, Bageac D, Danielian LE, Braun LE, Traynor BJ and Kwan JY (2016). "Longitudinal imaging in C9orf72 mutation carriers: Relationship to phenotype." Neuroimage Clin 12: 1035–1043. [PubMed: 27995069]

Floeter MK, Danielian LE, Braun LE and Wu T (2018). "Longitudinal diffusion imaging across the C9orf72 clinical spectrum." J Neurol Neurosurg Psychiatry 89(1): 53–60. [PubMed: 29054917]

Floeter MK, Traynor BJ, Farren J, Braun LE, Tierney M, Wiggs EA and Wu T (2017). "Disease progression in C9orf72 mutation carriers." Neurology 89(3): 234–241. [PubMed: 28615433]

Fortin JP, Parker D, Tunc B, Watanabe T, Elliott MA, Ruparel K, Roalf DR, Satterthwaite TD, Gur RC, Gur RE, Schultz RT, Verma R and Shinohara RT (2017). "Harmonization of multi-site diffusion tensor imaging data." Neuroimage 161: 149–170. [PubMed: 28826946]

Fox MD, Snyder AZ, Vincent JL, Corbetta M, Van Essen DC and Raichle ME (2005). "The human brain is intrinsically organized into dynamic, anticorrelated functional networks." Proc Natl Acad Sci U S A 102(27): 9673–9678. [PubMed: 15976020]

Jelsone-Swain LM, Fling BW, Seidler RD, Hovatter R, Gruis K and Welsh RC (2010). "Reduced Interhemispheric Functional Connectivity in the Motor Cortex during Rest in Limb-Onset Amyotrophic Lateral Sclerosis." Front Syst Neurosci 4: 158. [PubMed: 21228916]

Konrad C, Henningsen H, Bremer J, Mock B, Deppe M, Buchinger C, Turski P, Knecht S and Brooks B (2002). "Pattern of cortical reorganization in amyotrophic lateral sclerosis: a functional magnetic resonance imaging study." Exp Brain Res 143(1): 51–56. [PubMed: 11907690]

Lee SE, Sias AC, Mandelli ML, Brown JA, Brown AB, Khazenzon AM, Vidovszky AA, Zanto TP, Karydas AM, Pribadi M, Dokuru D, Coppola G, Geschwind DH, Rademakers R, Gorno-Tempini ML, Rosen HJ, Miller BL and Seeley WW (2017). "Network degeneration and dysfunction in presymptomatic C9ORF72 expansion carriers." Neuroimage Clin 14: 286–297. [PubMed: 28337409]

Leech R and Sharp DJ (2014). "The role of the posterior cingulate cortex in cognition and disease." Brain 137(Pt 1): 12–32. [PubMed: 23869106]

Li W, Zhang J, Zhou C, Hou W, Hu J, Feng H and Zheng X (2018). "Abnormal Functional Connectivity Density in Amyotrophic Lateral Sclerosis." Front Aging Neurosci 10: 215. [PubMed: 30065647]

Loewe K, Machts J, Kaufmann J, Petri S, Heinze HJ, Borgelt C, Harris JA, Vielhaber S and Schoenfeld MA (2017). "Widespread temporo-occipital lobe dysfunction in amyotrophic lateral sclerosis." Sci Rep 7: 40252. [PubMed: 28067298]

Lulé D, Diekmann V, Kassubek J, Kurt A, Birbaumer N, Ludolph AC and Kraft E (2007). "Cortical plasticity in amyotrophic lateral sclerosis: motor imagery and function." Neurorehabil Neural Repair 21(6): 518–526. [PubMed: 17476000]

Lule D, Ludolph AC and Kassubek J (2009). "MRI-based functional neuroimaging in ALS: an update." Amyotroph Lateral Scler 10(5-6): 258–268. [PubMed: 19922112]

Lulé DE, Müller HP, Finsel J, Weydt P, Knehr A, Winroth I, Andersen P, Weishaupt J, Uttner I, Kassubek J and Ludolph AC (2020). "Deficits in verbal fluency in presymptomatic C9orf72 mutation gene carriers-a developmental disorder." J Neurol Neurosurg Psychiatry 91(11): 1195–1200. [PubMed: 32855285]

Menke RA, Proudfoot M, Wuu J, Andersen PM, Talbot K, Benatar M and Turner MR (2016). "Increased functional connectivity common to symptomatic amyotrophic lateral sclerosis and those at genetic risk." J Neurol Neurosurg Psychiatry 87(6): 580–588. [PubMed: 26733601]

Menke RAL, Proudfoot M, Talbot K and Turner MR (2018). "The two-year progression of structural and functional cerebral MRI in amyotrophic lateral sclerosis." Neuroimage Clin 17: 953–961. [PubMed: 29321969]

Mohammadi B, Kollewe K, Samii A, Dengler R and Munte TF (2011). "Functional neuroimaging at different disease stages reveals distinct phases of neuroplastic changes in amyotrophic lateral sclerosis." Hum Brain Mapp 32(5): 750–758. [PubMed: 20836159]

Mohammadi B, Kollewe K, Samii A, Krampfl K, Dengler R and Munte TF (2009). "Changes of resting state brain networks in amyotrophic lateral sclerosis." Exp Neurol 217(1): 147–153. [PubMed: 19416664]

Murphy NA, Arthur KC, Tienari PJ, Houlden H, Chio A and Traynor BJ (2017). "Age-related penetrance of the C9orf72 repeat expansion." Sci Rep 7(1): 2116. [PubMed: 28522837]

Papma JM, Jiskoot LC, Panman JL, Dopper EG, den Heijer T, Donker Kaat L, Pijnenburg YAL, Meeter LH, van Minkelen R, Rombouts S and van Swieten JC (2017). "Cognition and gray and

white matter characteristics of presymptomatic C9orf72 repeat expansion." Neurology 89(12): 1256–1264. [PubMed: 28855404]

Renton AE, Majounie E, Waite A, Simon-Sanchez J, Rollinson S, Gibbs JR, Schymick JC, Laaksovirta H, van Swieten JC, Myllykangas L, Kalimo H, Paetau A, Abramzon Y, Remes AM, Kaganovich A, Scholz SW, Duckworth J, Ding J, Harmer DW, Hernandez DG, Johnson JO, Mok K, Ryten M, Trabzuni D, Guerreiro RJ, Orrell RW, Neal J, Murray A, Pearson J, Jansen IE, Sondervan D, Seelaar H, Blake D, Young K, Halliwell N, Callister JB, Toulson G, Richardson A, Gerhard A, Snowden J, Mann D, Neary D, Nalls MA, Peuralinna T, Jansson L, Isoviita VM, Kaivorinne AL, Holtta-Vuori M, Ikonen E, Sulkava R, Benatar M, Wuu J, Chio A, Restagno G, Borghero G, Sabatelli M, Heckerman D, Rogaeva E, Zinman L, Rothstein JD, Sendtner M, Drepper C, Eichler EE, Alkan C, Abdullaev Z, Pack SD, Dutra A, Pak E, Hardy J, Singleton A, Williams NM, Heutink P, Pickering-Brown S, Morris HR, Tienari PJ and Traynor BJ (2011). "A hexanucleotide repeat expansion in C9ORF72 is the cause of chromosome 9p21-linked ALS-FTD." Neuron 72(2): 257–268. [PubMed: 21944779]

Reuter M, Schmansky NJ, Rosas HD and Fischl B (2012). "Within-subject template estimation for unbiased longitudinal image analysis." Neuroimage 61(4): 1402–1418. [PubMed: 22430496]

Rittman T, Borchert R, Jones S, van Swieten J, Borroni B, Galimberti D, Masellis M, Tartaglia MC, Graff C, Tagliavini F, Frisoni GB, Laforce R Jr., Finger E, Mendonca A, Sorbi S, Rohrer JD and Rowe JB (2019). "Functional network resilience to pathology in presymptomatic genetic frontotemporal dementia." Neurobiol Aging 77: 169–177. [PubMed: 30831384]

Rohrer JD, Nicholas JM, Cash DM, van Swieten J, Dopper E, Jiskoot L, van Minkelen R, Rombouts SA, Cardoso MJ, Clegg S, Espak M, Mead S, Thomas DL, De Vita E, Masellis M, Black SE, Freedman M, Keren R, MacIntosh BJ, Rogaeva E, Tang-Wai D, Tartaglia MC, Laforce R Jr., Tagliavini F, Tiraboschi P, Redaelli V, Prioni S, Grisoli M, Borroni B, Padovani A, Galimberti D, Scarpini E, Arighi A, Fumagalli G, Rowe JB, Coyle-Gilchrist I, Graff C, Fallstrom M, Jelic V, Stahlbom AK, Andersson C, Thonberg H, Lilius L, Frisoni GB, Pievani M, Bocchetta M, Benussi L, Ghidoni R, Finger E, Sorbi S, Nacmias B, Lombardi G, Polito C, Warren JD, Ourselin S, Fox NC, Rossor MN and Binetti G (2015). "Presymptomatic cognitive and neuroanatomical changes in genetic frontotemporal dementia in the Genetic Frontotemporal dementia Initiative (GENFI) study: a cross-sectional analysis." Lancet Neurol 14(3): 253–262. [PubMed: 25662776]

Rooney J, Fogh I, Westeneng HJ, Vajda A, McLaughlin R, Heverin M, Jones A, van Eijk R, Calvo A, Mazzini L, Shaw C, Morrison K, Shaw PJ, Robberecht W, Van Damme P, Al-Chalabi A, van den Berg L, Chio A, Veldink J and Hardiman O (2017). "C9orf72 expansion differentially affects males with spinal onset amyotrophic lateral sclerosis." J Neurol Neurosurg Psychiatry 88(4): 281.

Schulthess I, Gorges M, Müller H-P, Lulé D, Del Tredici K, Ludolph AC and Kassubek J (2016). "Functional connectivity changes resemble patterns of pTDP-43 pathology in amyotrophic lateral sclerosis." Scientific reports 6.

Seeley WW (2017). "Mapping Neurodegenerative Disease Onset and Progression." Cold Spring Harb Perspect Biol 9(8).

Seeley WW, Crawford RK, Zhou J, Miller BL and Greicius MD (2009). "Neurodegenerative diseases target large-scale human brain networks." Neuron 62(1): 42–52. [PubMed: 19376066]

Shoukry RS, Waugh R, Bartlett D, Raitcheva D and Floeter MK (2020). "Longitudinal changes in resting state networks in early presymptomatic carriers of C9orf72 expansions." Neuroimage Clin 28: 102354. [PubMed: 32769055]

Smith SM, Jenkinson M, Johansen-Berg H, Rueckert D, Nichols TE, Mackay CE, Watkins KE, Ciccarelli O, Cader MZ, Matthews PM and Behrens TE (2006). "Tract-based spatial statistics: voxelwise analysis of multi-subject diffusion data." Neuroimage 31(4): 1487–1505. [PubMed: 16624579]

Sorrentino P, Rucco R, Jacini F, Trojsi F, Lardone A, Baselice F, Femiano C, Santangelo G, Granata C, Vettoliere A, Monsurrò MR, Tedeschi G and Sorrentino G (2018). "Brain functional networks become more connected as amyotrophic lateral sclerosis progresses: a source level magnetoencephalographic study." Neuroimage Clin 20: 564–571. [PubMed: 30186760]

Stanton BR, Williams VC, Leigh PN, Williams SC, Blain CR, Giampietro VP and Simmons A (2007). "Cortical activation during motor imagery is reduced in Amyotrophic Lateral Sclerosis." Brain Res 1172: 145–151. [PubMed: 17765211]

Tedeschi G, Trojsi F, Tessitore A, Corbo D, Sagnelli A, Paccone A, D'Ambrosio A, Piccirillo G, Cirillo M, Cirillo S, Monsurro MR and Esposito F (2012). "Interaction between aging and neurodegeneration in amyotrophic lateral sclerosis." Neurobiol Aging 33(5): 886–898. [PubMed: 20739098]

Trojsi F, Esposito F, de Stefano M, Buonanno D, Conforti FL, Corbo D, Piccirillo G, Cirillo M, Monsurro MR, Montella P and Tedeschi G (2015). "Functional overlap and divergence between ALS and bvFTD." Neurobiol Aging 36(1): 413–423. [PubMed: 25063233]

Trojsi F, Siciliano M, Femiano C, Santangelo G, Lunetta C, Calvo A, Moglia C, Marinou K, Ticozzi N, Ferro C, Scialò C, Sorarù G, Conte A, Falzone YM, Tortelli R, Russo M, Sansone VA, Chiò A, Mora G, Silani V, Volanti P, Caponnetto C, Querin G, Sabatelli M, Riva N, Logroscino G, Messina S, Fasano A, Monsurrò MR, Tedeschi G and Mandrioli J (2019). "Comparative Analysis of C9orf72 and Sporadic Disease in a Large Multicenter ALS Population: The Effect of Male Sex on Survival of C9orf72 Positive Patients." Front Neurosci 13: 485. [PubMed: 31156370]

Uddin LQ, Kelly AM, Biswal BB, Margulies DS, Shehzad Z, Shaw D, Ghaffari M, Rotrosen J, Adler LA, Castellanos FX and Milham MP (2008). "Network homogeneity reveals decreased integrity of default-mode network in ADHD." J Neurosci Methods 169(1): 249–254. [PubMed: 18190970]

van den Heuvel MP, Mandl RC, Kahn RS and Hulshoff Pol HE (2009). "Functionally linked resting-state networks reflect the underlying structural connectivity architecture of the human brain." Hum Brain Mapp 30(10): 3127–3141. [PubMed: 19235882]

Yeo BT, Krienen FM, Sepulcre J, Sabuncu MR, Lashkari D, Hollinshead M, Roffman JL, Smoller JW, Zollei L, Polimeni JR, Fischl B, Liu H and Buckner RL (2011). "The organization of the human cerebral cortex estimated by intrinsic functional connectivity." J Neurophysiol 106(3): 1125–1165. [PubMed: 21653723]

Zhou F, Gong H, Li F, Zhuang Y, Zang Y, Xu R and Wang Z (2013). "Altered motor network functional connectivity in amyotrophic lateral sclerosis: a resting-state functional magnetic resonance imaging study." Neuroreport 24(12): 657–662. [PubMed: 23839257]

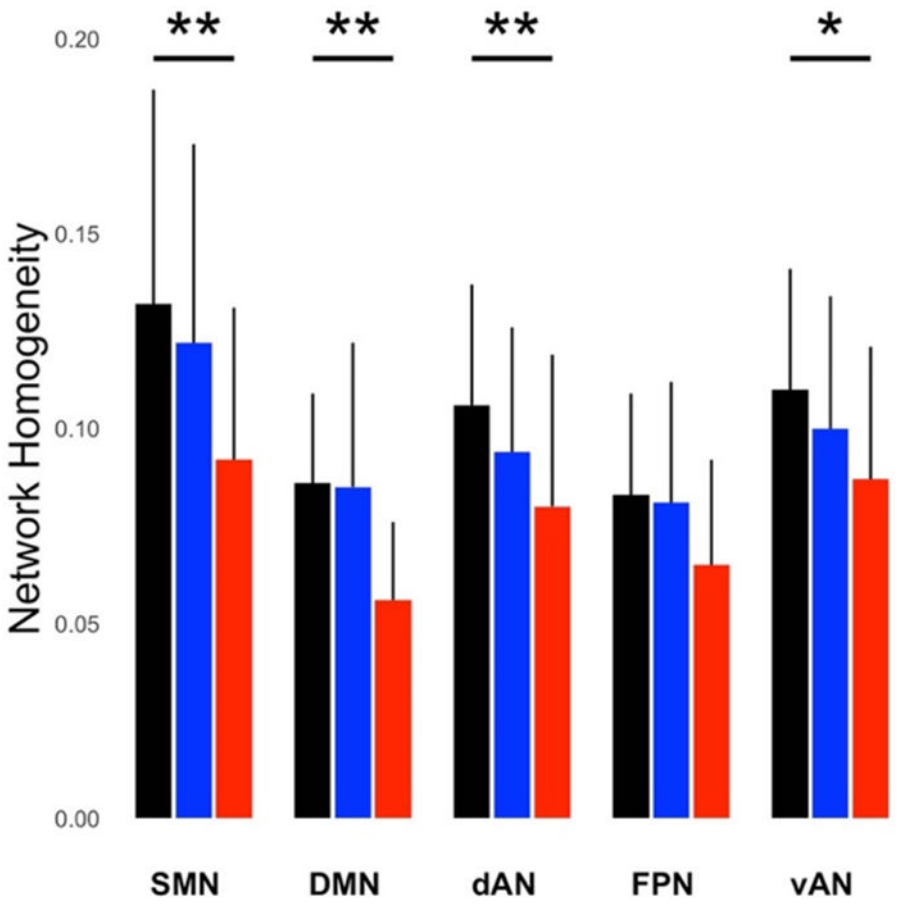

Figure 1.

Mean network homogeneity (NeHo) measures for five networks in healthy controls (black), presymptomatic C9+ carriers (blue), and symptomatic C9+ carriers (red), in a cross-sectional comparison using the last scan obtained from each person. NeHo is defined as the average correlation of all voxels within the network divided by the number of voxels in the network, using networks defined by Yeo et al (2011). NeHo was highest in healthy controls, followed by presymptomatic C9+ carriers, and symptomatic C9+ carriers. Asterisks indicate a significant linear relationship between diagnostic group and networks by Tukey's post-hoc test (* $p < 0.05$, ** $p < 0.01$). dAN = dorsal attention network; DMN = default mode network; SMN = somatomotor network; vAN = ventral attention network; FPN = frontoparietal network. Bars show group means and SD.

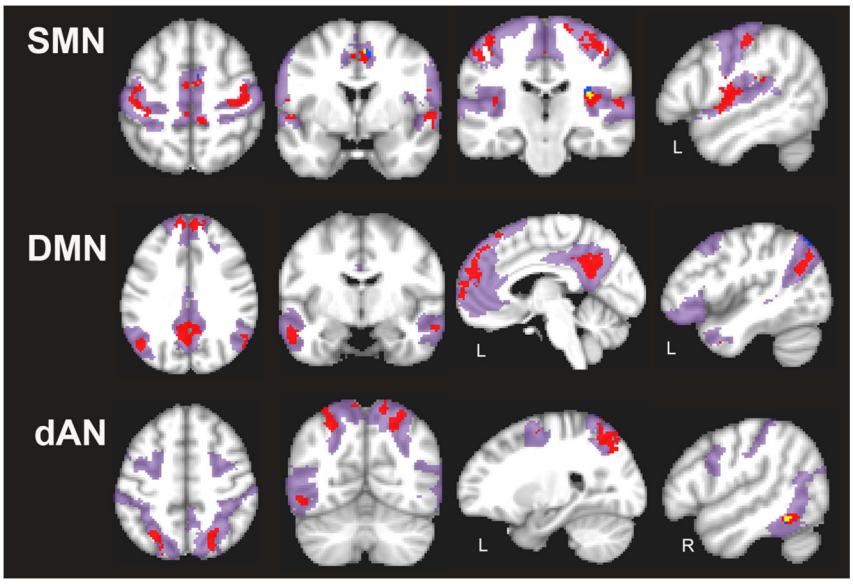

Figure 2.

Regions with reduced voxel-wise homogeneity in somatomotor (SMN), default mode (DMN) and dorsal attention (dAN) networks in C9+ carriers in a cross-sectional comparison using the last scan obtained from each person ($p < 0.05$ FWE corrected). Red = symptomatic C9+ carriers; blue = presymptomatic C9+ carriers; areas of overlap are shown in yellow. The extent of each network is shown in magenta shading. Left hemisphere is shown on the left in axial and coronal slices. Side of hemisphere is indicated for sagittal slices, L, left; R, right.

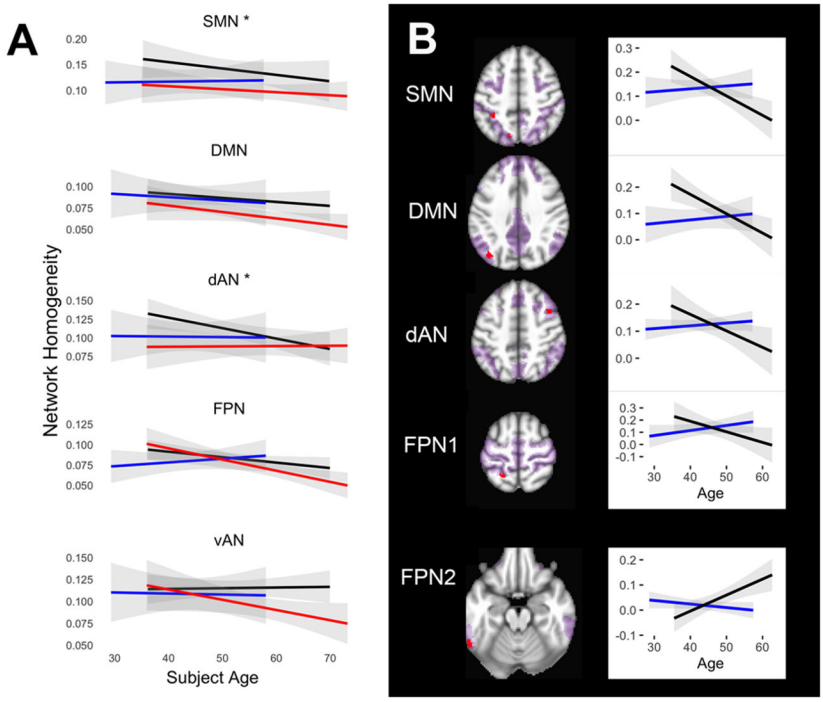

Figure 3.

Age-related changes in network homogeneity. **A)** Mean longitudinal trajectories of NeHo with age. Symptomatic C9+ carriers had reduced global homogeneity at all ages that continued to decline with age. Presymptomatic C9+ carriers diverged significantly from healthy controls in the somatomotor (SMN) and frontoparietal (FPN) networks. Black lines = healthy controls; red lines = symptomatic C9+ carriers; blue lines = presymptomatic C9+ carriers. Gray shading indicates 95% confidence interval, asterisks indicate networks with significant difference between groups ($p < 0.05$). **B)** Regions in networks in which the trajectory of changes in network homogeneity with age differed significantly between presymptomatic C9+ carriers (blue lines) and controls (black lines). Each graph shown with corresponding region in red to right ($p < 0.05$ FWE corrected). The top 4 graphs illustrate regions where presymptomatic carriers exhibited increasing homogeneity with age whereas controls declined. The bottom graph shows a region in the FPN (labeled FPN2) in which presymptomatic carriers had declining homogeneity but controls had increasing homogeneity. The extent of each network is shown in magenta. DMN = default mode network; dAN = dorsal attention network

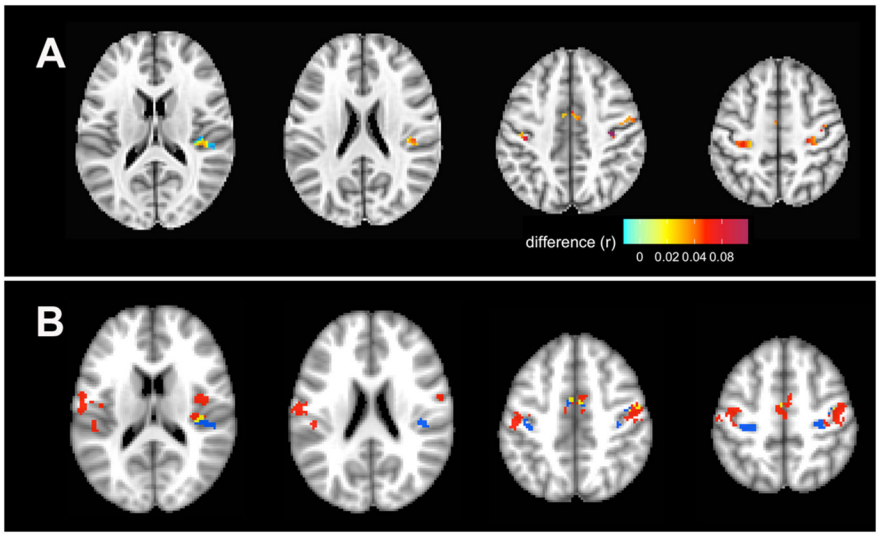

Figure 4.

Longitudinal increases in voxel-wise network homogeneity in the SMN in presymptomatic subjects. **A)** Regions with increasing network homogeneity ($p < 0.05$ FWE corrected). The color bar indicates the magnitude of the change in connectivity (r), with lighter colors indicating lesser change, and red indicating greater change. **B)** The same regions with increased network homogeneity as seen in panel A are shown here in blue to illustrate location of increased homogeneity in presymptomatic C9+ carriers relative to areas of decreased homogeneity in symptomatic C9+ carriers (red) at the time of their last scan, as in Figure 2. Yellow regions are areas of overlap.

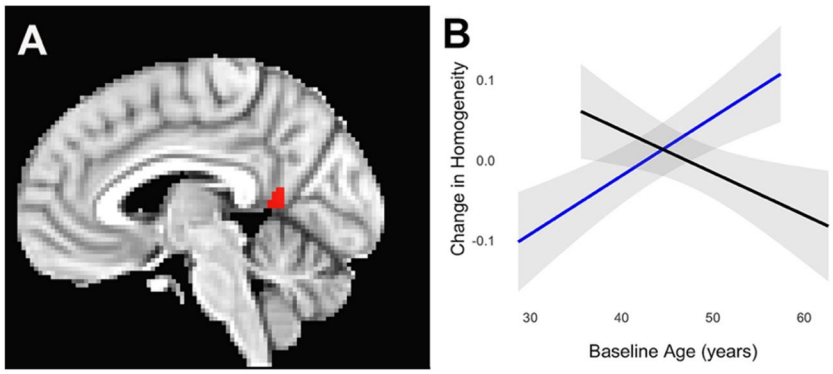

Figure 5.

Within the default mode network, the posterior cingulate (A, red region, $p < 0.05$ FWE corrected) exhibited a faster increase in homogeneity with age in presymptomatic C9+ carriers (B). Blue = presymptomatic carriers, black = controls. Gray shading indicates 95% confidence interval.

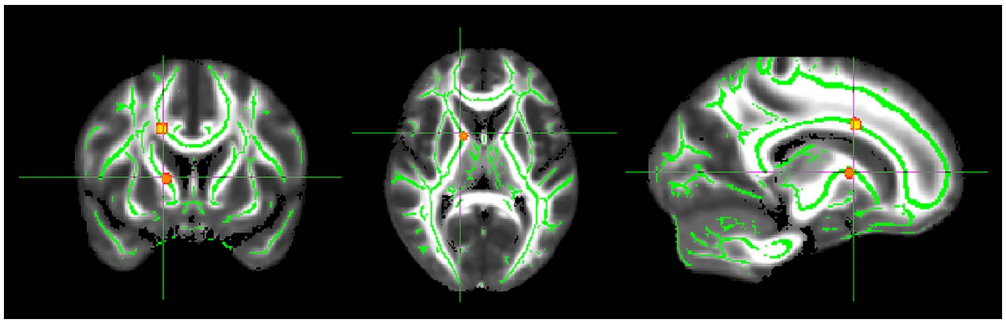

Figure 6.

Regions of white matter exhibiting reduced axial diffusivity in presymptomatic C9+ carriers between their first and final scan ($p < 0.05$ FWE corrected). The significant areas were thickened using the TBSS fill tool for better visualization.

Table 1.

Demographics of participants

	Healthy Controls	C9+ Symptomatic* carriers	C9+ Presymptomatic carriers
Age	51.4 ± 9.3	57.1 ± 9.8	43.4 ± 9.7[a]
% Male	53%	63%	20%
Symptom Duration (mos)		36.6 ± 25.1	
ALSFRS-R	48	35.9 ± 7.3	47.9 ± 0.4
Letter Fluency (words/letter) Baseline	14.3 ± 3.6 (n=22)	7.4 ± 4.1* (n=26)	12.7 ± 4.3
6-month follow-up	-	-	14.6 ± 4.3
18-month follow-up (N=12)	-	-	15.1 ± 3.4
Cross-sectional N	34	27	15
Interval (N with 2 scans)	4.85 ± 2.79 (N=21)	5.87 ± 0.74 (N =17)	5.71 ± 1.17 (N=14)
Interval (N with 3 scans)	18.31 ± 2.11 (N=21)	17.94 ± 0.92 (N= 8)	18.25 ± 1.17 (N=13)

[a] C9+ presymptomatic < HC and C9+ symptomatic, ANOVA p<0.05 corrected

* 17 ALS/6 ALS-FTD/4 Dementia

Table 2.

Regions with reduced intra-network homogeneity in C9+ carriers compared to healthy controls.

	% voxels/network with reduced homogeneity		Location of areas* with reduced voxel-wise homogeneity	
Network	**Symptomatic**	**Presymptomatic**	**Symptomatic**	**Presymptomatic**
SMN	11.75	0.3	L/R Precentral, L/R Postcentral, L/R Medial Frontal, L/R Paracentral, L/R Cingulate	R Precentral, R Medial Frontal
DMN	9.54	0.09	L/R Precuneus, L/R Angular, L/R Middle Temporal, L/R Sup. Frontal	L Superior Parietal
dAN	7.25	0.11	L/R Precuneus, R Postcentral, R Middle Temporal, R Fusiform, L Middle Occipital	R Middle Temporal
vAN	3.64	0	R Paracentral, R Cingulate, R Inferior Parietal, R Insula, L Precentral	-
FPN	1.71	0	L/R Mid. Frontal, R Superior Parietal, L Inferior Parietal	-

*Atlas of Desikan et al 2006; voxel-wise measures of intra-network homogeneity; L left, R right; L/R bilateral; networks of interest (SMN = sensorimotor, DMN = default mode; dAN = dorsal attention network, vAN ventral attention network, FPN frontoparietal network.

Table 3.

Longitudinal change in direction of correlation of voxels with significant changes in homogeneity in the somatomotor network of presymptomatic C9orf72 mutation carriers

	Anticorrelated		Correlated	
	Less than −0.1	**0 to −0.1**	**0 to 0.1**	**More than 0.1**
	Change in mean value of functional connectivity (%)			
Session 1 vs. 2	0.68	0.46	0.74	5.07
Session 1 vs. 3	−3.49	1.02	2.17	13.34
	Number of connections to total connections (%)			
Session 1	17	15	18	50
Session 2	16	13	17	54
Session 3	13	11	15	61